Temporal–spatial diversities of long-range correlation for relative humidity over China

Guangxing Lin[a], Xi Chen[a], Zuntao Fu[a,b],*

[a]*School of Physics, Peking University, Beijing 100871, China*
[b]*State Key Laboratory for Turbulence and Complex Systems, Peking University, Beijing 100871, China*

Abstract

Long-range correlations of daily relative humidity anomaly records from 191 weather stations over China during 1951–2000 are analyzed by means of fluctuation analysis (FA) and detrended fluctuation analysis (DFA). The information about trends in the relative humidity records can be obtained by comparing the FA curve with DFA curves. The daily relative humidity fluctuations are found to be power-law correlated and their average scaling exponent is higher than that of the temperature fluctuations, indicating that the relative humidity fluctuations take different statistical behavior from other meteorological quantities and there exists a stronger persistence in the relative humidity fluctuations. Furthermore, it is also found that these power-law scaling properties vary from station to station and show both spatial and temporal diversities, which may be explained by a proposed mechanism.
© 2007 Elsevier B.V. All rights reserved.

Keywords: Relative humidity; Fluctuation analysis; Detrended fluctuation analysis; Scaling exponent

1. Introduction

Long-range correlations within the climate system are of physical and practical interest. A cold day is usually followed by a cold day, and a warm day is more likely to be followed by a warm day. On a large scale of about one week, there is typical short-time persistence, since the general weather system lasts for about seven days. Furthermore, the El Niño-southern oscillation event, one of the most significant phenomena, occurs every 3–5 years and strongly affects the weather over the tropical Pacific as well as North America. Therefore, the analysis of correlations within the different climatic compartments of the climate system is fundamental in climate research. But as the longer time scales are often governed by different process like circulation patterns and even associated with different trends like global warming [1,2], defining long-term correlations becomes more difficult. To address this problem, detrended fluctuation analysis (DFA for short) was developed to accurately quantify long-range power-law correlations embedded in a nonstationary time series [3,4]. Recently, the DFA method has been successfully applied to meteorological data [5–10]. In Ref. [6]

---

*Corresponding author. School of Physics, Peking University, Beijing 100871, China.
E-mail address: fuzt@pku.edu.cn (Z. Fu).

daily noon temperatures of several meteorological stations were analyzed by means of DFA. The resulting scaling of the variability implies that the temperature auto-correlation $C(s)$ decays as power law, $C(s) \sim s^{-\gamma}$ with roughly the same exponent $\gamma = 0.7$. This exponent of about $\frac{2}{3}$ was also confirmed to characterize daily maximum temperatures in a range of times between 10 days and at least 25 years [7]. In Ref. [8], DFA was applied to study temperature correlations in the sea surface temperatures (SSTs). It was found that the temperature auto-correlation function $C(s)$ again decayed by a power law, but with an exponent close to 0.4, indicating a stronger persistence in the oceans than in the continents.

In this paper, we study the fluctuations of relative humidity (R-H for short) records at 191 weather stations over China mainly using DFA. The study indicates that the daily R-H fluctuations over all stations show power-law correlations, with a higher scaling exponent than that of temperature fluctuations, which shows that the R-H fluctuations take different statistical behavior from other meteorological quantities, such as temperature. And the rest of this article is organized as follows. In Section 2, the methods used in this paper: FA and DFA are outlined and the data sets are described. Long-range correlation analysis for fluctuations of R-H over 191 stations and their geographical distribution are presented in Section 3. Finally, Section 4 concludes the paper.

2. Methodology and data

2.1. Methodology outline

Consider a fluctuating time series x_i ($i = 1, \ldots, N$) sampled at equidistant times $i\Delta t$. Quantitatively, the persistence in the time series can be characterized by its auto-correlation function

$$C(s) = <(x_i - \bar{x})(x_{i+s} - \bar{x})> = \frac{1}{N-s} \sum_{i=1}^{N-s} (x_i - \bar{x})(x_{i+s} - \bar{x}), \tag{1}$$

where N is the length of the time series, s is the time lag and $\bar{x}$ denotes the mean value of the time series. A direct calculation of $C(s)$ is usually not appropriate due to the noise presenting in the finite time series and underlying trends of unknown origins. Thus, instead of calculating the auto-correlation function directly, the profile of the time series

$$Y_i = \sum_{k=1}^{i} x_k - \bar{x}, \tag{2}$$

is calculated firstly, then it is divided into non-overlapping segments of equal length s indexed by $k = 1, \ldots, N_s$ with $N_s = [N/s]$. Since the record length N is not always a multiple of the segment length s, there often remains a short part left at the end of the profile. In order to keep this part of the profile, the same procedure is repeated from the other end of the record. Therefore, $2N_s$ segments are obtained altogether. Next we calculate the square fluctuation $F_s^2(k)$ in each segment, which can be calculated by two ways. In the fluctuation analysis (FA), the square fluctuation $F_s^2(k)$ in the kth segment is identified as the square of difference between the values of the profile at the beginning and the end of the segment, $F_s^2(k) = (Y_{(k+1)s} - Y_{ks})^2$. In the DFA, the local trend for each kth segment is calculated by a least-squares fit and the corresponding square fluctuation $F_s^2(k)$ is defined as the variance of the original profile subtracted from the best fit in the segment. Different orders n of DFA (DFA1, DFA2, etc.) differ in the order of the polynomial used in the fitting procedure (for more details, see Ref. [11]). And then the root-mean-square fluctuations $F(s)$ is obtained by averaging over all segments of size s,

$$F(s) = \left[\frac{1}{2N_s} \sum_{k=1}^{2N_s} F_s^2(k) \right]^{1/2}. \tag{3}$$

For the case of long-range power-law correlations, $F(s)$ will increase asymptotically with s by a power-law

$$F(s) \sim s^{\alpha}, \tag{4}$$

where $0 < \alpha < 1$. Notice that such a process has also a power-law auto-correlation function

$$C(s) \sim s^{-\gamma},\tag{5}$$

the relationship between the correlation exponents is [5,9]

$$\gamma = 2(1 - \alpha).\tag{6}$$

Consequently, long-memory (persistent) process is characterized by an exponent $\alpha > 0.5$, uncorrelated time series obey $\alpha = 0.5$, antipersistent signals showing negative long-range correlations have $\alpha < 0.5$.

In this article, we employ two different methods i.e., FA and DFA to measure the fluctuations and to eliminate possible trends. According to the definition above, the method of FA cannot rule out the trends imposed on the time series, while DFAn eliminates trends of order n in the profile and $n - 1$ in the original time series. Therefore, we can learn about long-term correlations and detect the influence of trends or other nonstationarities by comparing the root-mean-square fluctuation $F(s)$ obtained from different methods (for general discussion, see Refs. [11–13]).

2.2. Data sets

The records used in this paper were obtained from a high-quality daily surface climatic data sets, processed by Chinese National Meteorological Information Center (NMIC), of 194 Chinese meteorological stations taking part in international exchange. The same collection was utilized in many studies to analyze climate change over China in the recent 50 years [14,15]. Data for three stations, station 54618, 52203 and 54909, were kicked out because of their short time span about only 10 years, while records of the other stations last about 50 years, from 1951 to 2000. According to Ref. [12], scaling of correlated data series are not affected by randomly cutting out segments and stitching together the remaining parts, even when 50% of the points are removed. Therefore we remove the missing values from the raw data over some stations, since they are only a little part of series. The main data sets used in this paper are R-H time series, where R-H is defined as [16]

$$e = \frac{p_v}{p_{sat}(T)} 100\%,\tag{7}$$

where the partial vapor pressure p_v of gaseous water in the air is used to quantify the air humidity. At a given temperature T, the amount of water in the air is limited. The maximum partial vapor pressure corresponding the maximum water content is the saturation vapor pressure $p_{sat}(T)$.

To overcome the natural nonstationarity of the R-H and temperature data due to season trends, we remove the annual cycle from the raw data e_i (R-H) or T_i (daily mean temperatures) by computing the anomaly series $e_i' = e_i - \langle e_i \rangle_d$ for R-H or $T_i' = T_i - \langle T_i \rangle_d$ for temperatures, where $\langle \ \rangle_d$ denotes the long-time average value for the given calendar day.

3. Long-range correlation analysis for relative humidity and geographical distribution

First of all, let us study single R-H series of two stations: station Tianjin in the north of China and station Shantou in the south of China. Fig. 1(a) and (c) show the profile for station Tianjin and Shantou, respectively. It is obvious that there exist different shapes in these profiles: Fig. 1(a) first fluctuates above the value 0 and then decreases below 0, taking a shape just like the letter "z", while Fig. 1(c) fluctuates above 0 all the time and shows parabolic-like shape, which may indicate the presence of a negative linear trend. To detect the trend further, we examine their FA and DFA results (see Fig. 1(b) and (d)). In Fig. 1(b) both the FA curve and DFA curves are approximately straight lines over all ranges, which have the same slope about 0.70 ± 0.02. In contrast to Fig. 1(b), the curves of Fig. 1(d) show some diversities: slopes of FA curve and DFA curves are different and crossovers exist in all curves—the value of the scaling exponent differs for different ranges of scales. It is obvious that the slope of the FA curve is larger than that of DFA curves: the FA curve increases sharper than DFA curves, especially after the scale of 100 days. And this fact indicates the existence of trends by which the long-term correlations are masked in the FA result. Calculation using FA alone will yield a higher correlation exponent and thus lead to a spurious overestimation of the long-term persistence (for a

a

b

c

d

e

f

g

h
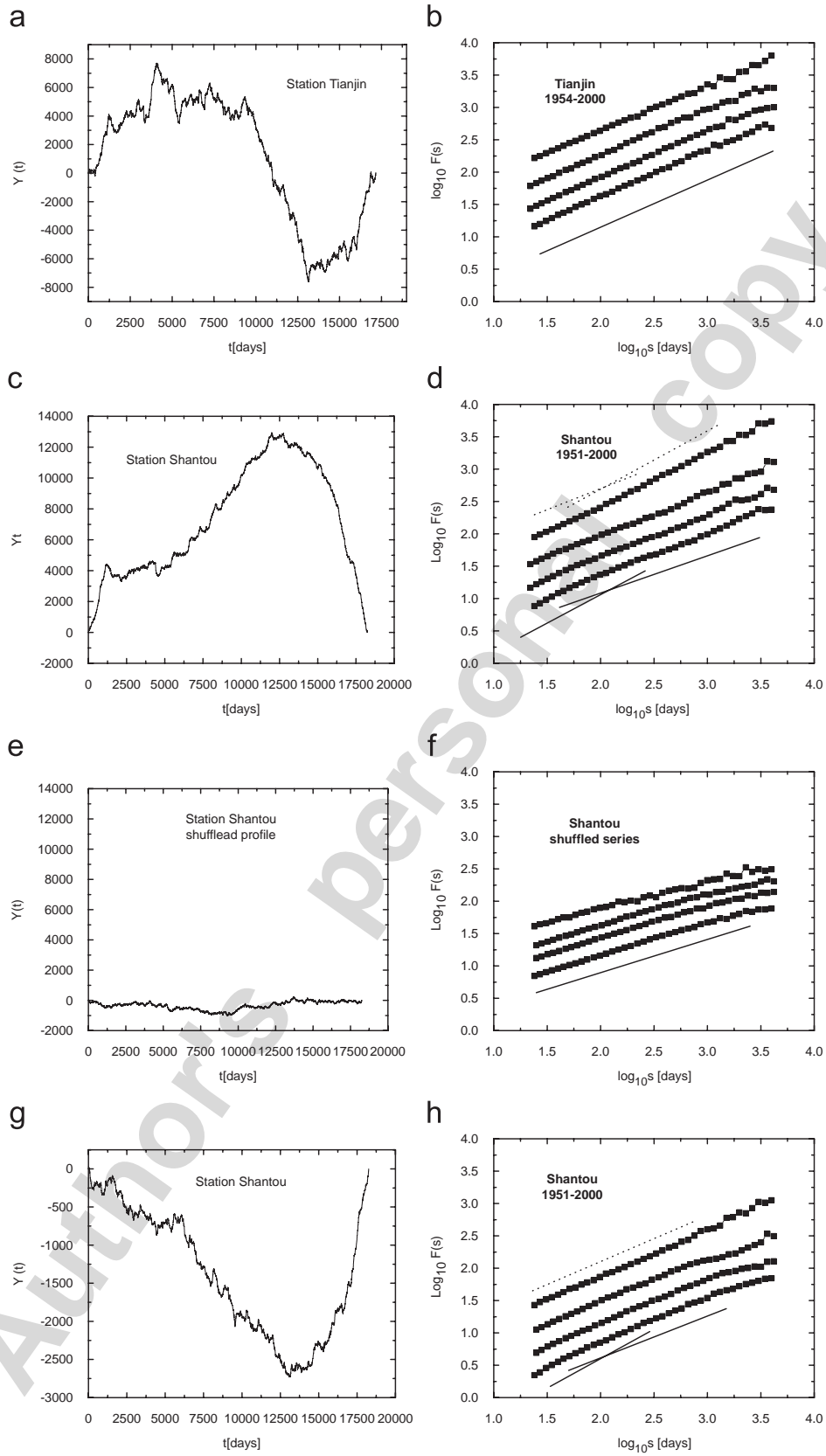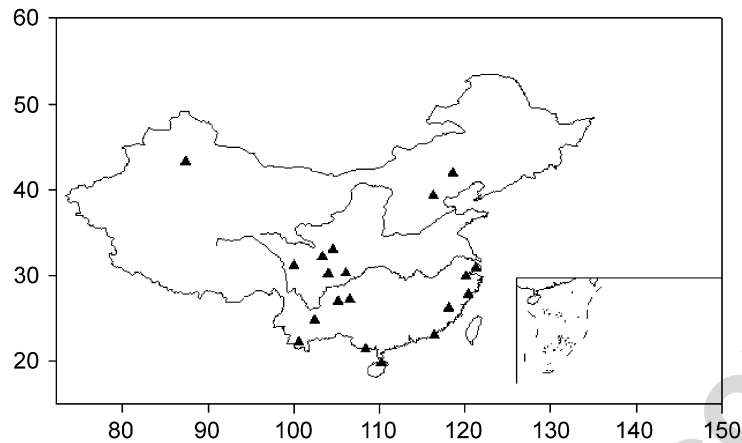
Fig. 2. The stations that show a pronounced negative linear trend of R-H in 1951–2000 have been marked with solid triangles.

general discussion, see Refs. [11,13]). The phenomenon that the DFA2 curve and DFA3 curve show the same shape and slope suggests that there are no significant nonlinear trends imposing on the R-H time series of station Shantou. Moreover, different from station Tianjin, all DFA curves do not exhibit constant slope (scaling exponent) for all ranges. The R-H fluctuation scaling exponent on small scale below nearly 100 days ($\alpha \approx 0.80 \pm 0.01$) higher than that on large scale from about 100 to 1000 days ($\alpha \approx 0.61 \pm 0.01$) shows a crossover existence (due to the lack of statistical significance, the curves above 1000 days should not be taken into account [13], and thus the same way will be adopted in the following article). In this point, we should point out that although there also exists a crossover in DFA curves of both land atmospheric temperatures and SSTs [5,6,8], crossover of land atmospheric temperatures occurs roughly at $s_x = 10$ days, which is the order of magnitude for a typical so-called "general weather regimes", and crossover of SSTs occurs at about $s_x = 10$ months.

For a further confirmation of our findings that higher scaling exponent in the FA treatment than in the DFA treatment is due to linear trend and the existence of crossover in DFA curves is due to different correlations in different ranges, but not due to a broad probability distribution [17], we have eliminated the trends and correlations by randomly shuffling the R-H data for station Shantou. This shuffling has no effect on the probability distribution function of the R-H data. Fig. 1(e) and (f) show the profile and results of both FA and DFA for the shuffled data, respectively. It is obvious that there is no crossover and the slopes of the FA curve and DFA curves are both about 0.5 just as expected, confirming our findings.

Since the results of FA and DFA for station Tianjin and Shantou show so significant differences, we are interested in the difference of linear trends and correlations of different time scales between weather stations over China. Fig. 2 shows the weather stations of which the scaling exponent of the FA curve of daily R-H series is at least 0.05 larger than that of DFA3 curve (since all DFA curves show nearly the same slope, we chose the DFA3 with caution) in the range from 100 to 1000 days, suggesting that there exist pronounced linear trends in daily R-H series for these weather stations. According to the convex profiles just like Fig. 1(c), we can conclude that the daily R-H records exhibit a decreasing trend for these weather stations and thus in recent 50 years there is a tendency to become drier most in two regions: near the coastline of southern and

Fig. 1. (a) The R-H profile for Tianjin during 1954–2000. (b) Log–log plots of the FA and DFA curves of the R-H for Tianjin, from top to bottom curves correspond to FA, DFA1, DFA2 and DFA3, where the curves are shifted for clarity and the solid line is guideline slope of the FA and DFA curves, its slope is 0.70 ± 0.02. (c) and (d) The analogs to (a) and (b) but for Shantou, where the dot lines and solid lines are guideline slopes of the FA and DFA curves, respectively. Their slopes are 0.74 ± 0.01 (on small scale for the FA curve), 0.84 ± 0.01 (on large scale for the FA curve), 0.80 ± 0.01 (on small scale for the DFA curves) and 0.61 ± 0.01 (on large scale for the DFA curves). (e) and (f) The analogs to (a) and (b) but for randomly shuffled daily R-H series over Shantou. The slope is 0.49 ± 0.02. (g) and (h) The analogs to (c) and (d) but for daily temperature series over Shantou. The slopes are 0.73 ± 0.01 (for the FA curve), 0.82 ± 0.01 (on small scale for the DFA curves) and 0.69 ± 0.01 (on large scale for the DFA curves).
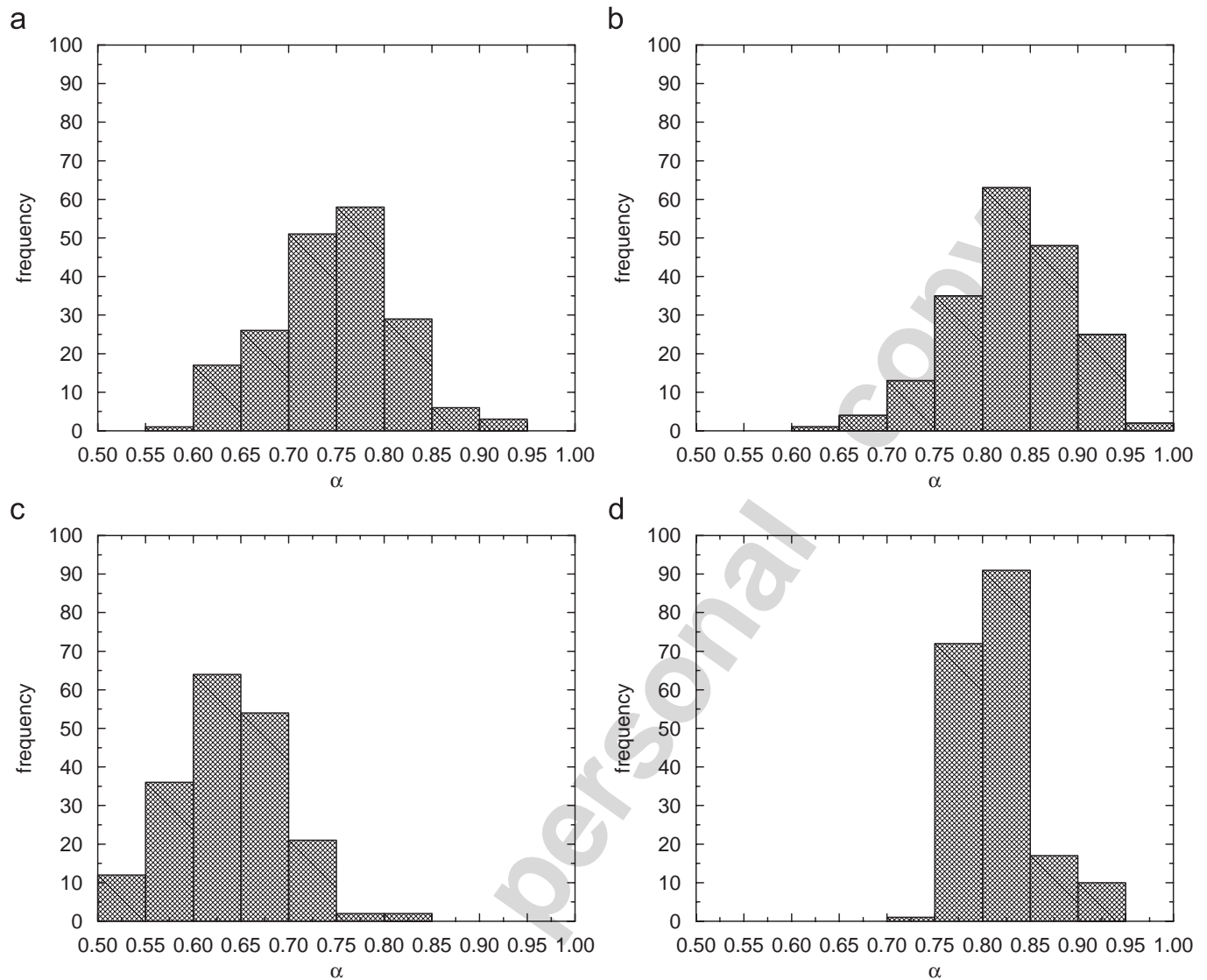
Fig. 3. The histogram of the scaling exponents. (a) For R-H fluctuations on the large time scale from 100 to 1000 days. (b) For R-H fluctuations on the small time scale below 100 days. (c) For temperature fluctuations on the large time scale from 100 to 1000 days. (d) For temperature fluctuations on the small time scale below 100 days.

eastern China and Sichuan Basin between the upper Yangtze River valley and the upper Yellow River valley. In the former region, this drier tendency is partly caused by the trend of increasing temperature [18], due to urban warming. We check the daily temperature series for the station Shantou, as an example. The concave profile in Fig. 1(g) may reflect a positive linear trend, and the higher long-term scaling exponent of FA result, $\alpha \approx 0.73 \pm 0.01$ than that of DFA results, $\alpha \approx 0.69 \pm 0.01$ in Fig. 1(h) confirms that warming trend. However, the warming trend in recent 50 years is not found in the region of Sichuan Basin, and we attribute the drier tendency mostly to the trend of decreasing precipitation [14,19]. What is surprising, in North of China, where many researchers found there were dry signs during the time from 1951 to 1999 [15,20], we do not detect significant drier trend through the methods of FA and DFA except for only two stations.

Then we study the distribution of the DFA scaling exponents over 191 weather stations. Fig. 3(a) and (b) show the statistical histogram for the values of the scaling exponent α obtained by DFA3 from R-H time series ranging from 100 to 1000 days and below 100 days, respectively. For the small scale below 100 days, the average exponent is $\alpha_s \approx 0.83 \pm 0.06$, while the average exponent $\alpha_l \approx 0.75 \pm 0.07$ for the large scale from 100 to 1000 days. Compared to the average scaling exponent of land temperature series $\alpha \approx 0.65$ [5,7], the daily R-H time series exhibit a much stronger correlation at least on the time scale from 100 to 1000 days. In fact,
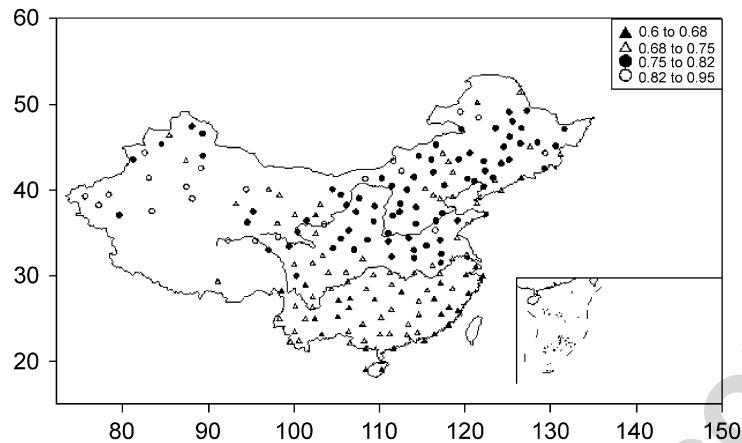
Fig. 4. The geographical distribution of scaling exponents α of daily R-H on the scale from 100 to 1000 days for 191 stations over China.

we can get the same conclusion from DFA3 results of daily temperature records shown in Fig. 3(c) and (d) for the 191 weather stations over China. Similar to Fig. 3(a) and (b), Fig. 3(c) and (d) show the statistical histogram for the values of the scaling exponent α in the range from 100 to 1000 days and below 100 days, respectively, but for daily temperature records. While the average small-scale exponent $\alpha_s \approx 0.81 \pm 0.04$ is near the same as daily R-H records, the average large-scale exponent $\alpha_l \approx 0.64 \pm 0.06$ is much smaller than that of daily R-H records, proving that stronger temporal correlations in R-H fluctuations than in temperature fluctuations, which indicates that the R-H fluctuations have different statistical behavior from other meteorological quantities [16]. Moreover, it is obvious that for many stations the daily R-H series exhibit stronger persistence for small-scale than that for large-scale.

Furthermore, from Fig. 3 we can learn that the scaling exponent is not universal but different from station to station. Fig. 4 shows the geographical distribution of the scaling exponents over China in the range from 100 to 1000 days. South China and Southwest China show $\alpha < 0.75$, below the average scaling exponent, whereas the rest of China, North China, Northwest China and Northeast of China, reveals a distinct increase, $\alpha > 0.75$, above the average scaling exponent. Especially, the higher scaling exponent $\alpha > 0.82$ in Northwest of China is compared sharply with the lower scaling exponent $\alpha < 0.68$ in Southwest of China and coastal line of South China. Accordingly, there is no universal scaling behavior since the large-scale exponents vary strongly from station to station and this reflects that there exist different mechanisms for R-H long-term persistence in different regions. This is in contrast to climate data, where universal long-term persistence of temperature records at land stations was observed [5,7,21,22]. This different persistence depending on geography may be attributed partly to the different interannual rainfall variability. It is well known that the value of R-H in one region is much related to the rainfall frequency in this region: the more frequent rainfall, the larger R-H usually, and vice versa. And since the standard deviation is a measure of fluctuations to some extent, the geographical distribution of standard deviations of the rainfall anomaly series (profile) is plotted in Fig. 5. These standard deviations are calculated over the whole record where each data point consists of an annual total of daily rainfalls. Since the average standard deviations over 191 stations is about (153.7 ± 101.2) mm, we divide these stations into four regions. The values are different between the south and the north of Yangtze River quite similar to Fig. 4 and the smallest (largest) standard deviations in Fig. 5 corresponds well to the largest (smallest) scaling exponents in Fig. 4 in Northwest China (South China). Therefore, the contribution of larger interannual rainfall variability may be lead to less long-term correlated R-H series, but more comprehensive studies will be needed to confirm this interesting result.

In order to reflect the difference of large-scale and small-scale correlation behavior of daily R-H series, the value of small-scale scaling exponent minus the value of large-scale scaling exponent to derive $\Delta\alpha = \alpha_s - \alpha_l$ for each weather station is to plot Fig. 6. Similar to Fig. 4, values in the north of China are different from values in the south of China, but values in the north of China are smaller than that in the south of China, indicating that the scaling properties of the daily R-H series for the north of China change a little compared with the south of
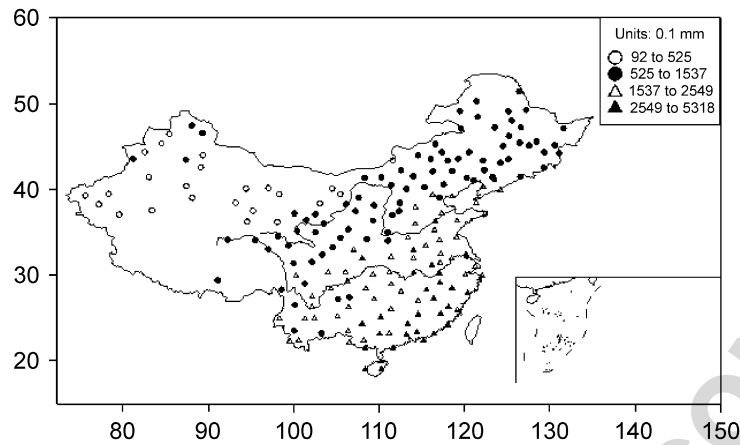
Fig. 5. The geographical distribution of standard deviations σ of the yearly rainfall fluctuations for 191 stations over China.
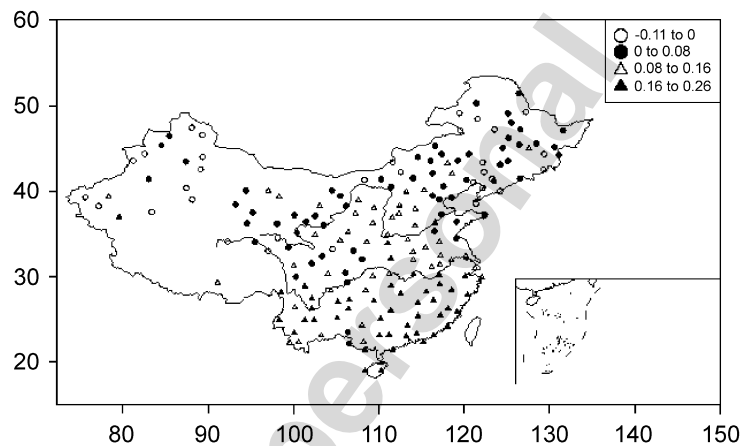
Fig. 6. The geographical distribution of difference between scaling exponents over small scale and large scale $\Delta\alpha = \alpha_s - \alpha_l$ of daily R-H for 191 stations over China.

China in the range below 1000 days. Again, this difference may be attributed to the rainfall frequency. In the south of China, there usually exists a rainy season, so-called Meiyu, roughly from Mid-May to Mid-August, leading to a stronger persistence on the scale of below season (nearly 100 days): it is usual to rain in the rainy season for weeks and even longer and not to rain in the other time in one year, and thus the daily R-H anomaly series show a stronger persistence on the scale of below 100 days than that in large-scale. In the north of China, especially in Northwest China, most rain does not fall in some fixed time range but randomly, therefore there is no significant stronger small-scale persistence than large-scale persistence, and even more, this random rainfall shuffle the small-scale persistence of R-H fluctuations and lead to smaller small-scale scaling exponents than large-scale scaling exponents at some weather stations.

As it is reported, the various climates of China are major determined by the system of the East Asian summer and winter monsoon forced by the thermal effect of land–sea contrast and the elevated heat source produced by the huge massif of the Tibetan Plateau [23–28]. The climate in western China is generally very dry, but it is mainly semi-humid and humid in the eastern part of the country. After the onset of the East Asian summer monsoon, the moisture transport coming from Indochina Peninsula and the South China Sea leads to the commencement of rainy season. With the northward match of the monsoon system, the monsoon rainy belt crosses the region from the South China in the early May to the Yangtze River Basin in Mid-June and finally to the North China in the late July, leading to a dramatic change in climate regime in these regions [29,30]. But due to changes in Eurasian or Tibetan snow cover and the Pacific SST [31–33], the East Asian summer monsoon and related seasonal rain belts assumes significant variability at intraseasonal, interannual and interdecadal time scales. These multi-time scales rainy belt variabilities are just corresponding to the

interannual rainfall variability and the seasonal rain mentioned in the last two paragraphs. Therefore, from the fact that the different R-H fluctuation scaling exponents are related to different rainfall variabilities, and that the rainfall variabilities are caused by East Asian Summer monsoon system, the different R-H fluctuation scaling exponents may reflect the different physical processes and mechanisms controlling the different climate regions over China, and further it is useful to exploit the fluctuation scaling exponent for an indicator of different climate regions.

4. Conclusion and discussion

In this paper, we have studied daily R-H records for about 50 years for 191 weather stations over China by using the methods of FA and DFA. The main results of the study are the following.

A linear trend imposing on the R-H fluctuations have been detected by comparing the FA curve with the DFA3 curve. While in some stations near the coastline of southern and eastern China and Sichuan Basin between the upper Yangtze River valley and the upper Yellow River valley, we did see the indications for trends of decreasing R-H, we did not find pronounced linear trends in most of weather stations over China. This fact may indicate that there is no pronounced tendency to become drier or wetter in the vast majority of stations over China and that the actual drier tendency in North of China in the recent 50 years is less pronounced than that found before [15,20].

The daily R-H variations are correlated and can be characterized by power-law correlations, just as the temperature fluctuations, at least in the range below 1000 days. And the fact of the higher average scaling exponent for R-H fluctuations than that for temperature fluctuations shows that the R-H fluctuations have a stronger persistence than the temperature fluctuations. Moreover, the persistence of R-H fluctuations exhibits both temporal and spatial diversities. In the spatial respect, the scaling exponents exhibit a broad distribution, varying from about 0.55 to near 1.0 in different weather stations of China, in contrast to the universal exponent of the temperature fluctuations $\alpha \approx 0.65$ [5,7,21,22]. And the scaling properties are different from station to station: for some stations in the north of China the fluctuations show the constant exponent on all time scales, while for other stations in the south of China there exists a crossover roughly at the time of 100 days. The crossover reflects an important change in the dynamical behavior of the daily R-H fluctuations between the time scale of below 100 days and from 100 to 1000 days, and this is the temporal diversity for the R-H fluctuations.

For explaining these diversities, an effecting factor is suggested: rainfall variability. The difference of large-scale scaling exponents for the R-H fluctuations is partly caused by the difference of annual rainfall variability between stations over China. And the rain season in the south of China probably causes the stronger small-scale correlation than large-scale correlation of the R-H fluctuations, while the random rainfall in the north of China is very likely to shuffle the small-scale correlation of the R-H fluctuations. But more comprehensive studies will be needed to confirm this interesting issue.

Acknowledgment

References

[1] A.G. Dai, K.E. Trenberth, T.R. Karl, Geophys. Res. Lett. 25 (1998) 3367.
[2] P.M. Zhai, X.H. Pan, Geophys. Res. Lett. 30 (2003) 1913.
[3] C.K. Peng, S.V. Buldyrev, S. Havlin, M. Simons, H.E. Stanley, A.L. Goldberger, Phys. Rev. E 49 (1994) 1685.
[4] M.S. Taqqu, V. Teverovsky, W. Willinger, Fractals 3 (1995) 785.
[5] J.F. Eichner, E. Koscielny-Bunde, A. Bunde, S. Havlin, H.J. Schellnhuber, Phys. Rev. E 68 (2003) 046133.
[6] E. Koscielny-Bunde, A. Bunde, S. Havlin, Y. Goldreich, Physica A 231 (1996) 393.
[7] E. Koscielny-Bunde, A. Bunde, S. Havlin, H.E. Roman, Y. Goldreich, H.J. Schellnhuber, Phys. Rev. Lett. 81 (1998) 729.
[8] R.A. Monetti, S. Havlin, A. Bunde, Physica A 320 (2003) 581.
[9] A. Tsonis, P.J. Roebber, J.B. Elsner, Geophys. Res. Lett. 25 (1998) 2821.

[10] A. Tsonis, P.J. Roebber, J.B. Elsner, J. Clim. 12 (1999) 1534.
[11] J.W. Kantelhardt, E. Koscielny-Bunde, H.A. Rego, S. Havlin, A. Bunde, Physica A 295 (2001) 441.
[12] Z. Chen, P.Ch. Ivanov, K. Hu, H.E. Stanley, Phys. Rev. E 64 (2002) 041107.
[13] K. Hu, P.Ch. Ivanov, Z. Chen, P. Carpena, H.E. Stanley, Phys. Rev. E 64 (2001) 011114.
[14] P.M. Zhai, X.B. Zhang, H. Wan, X.H. Pan, J. Clim. 18 (2004) 1096.
[15] X.K. Zou, P.M. Zhai, Q. Zhang, Geophys. Res. Lett. 32 (2005) L04707.
[16] G. Vattay, A. Harnos, Phys. Rev. Lett. 73 (1994) 768.
[17] E. Koscielny-Bunde, J.W. Kantelhardt, P. Braun, A. Bunde, S. Havlin, J. Hydrol. 322 (2006) 120.
[18] W.H. Qian, X. Lin, Clim. Res. 27 (2004) 119.
[19] W.H. Qian, X. Lin, Meteorol. Atmos. Phys. 90 (2005) 193.
[20] J.P. Yang, Y.J. Ding, R.S. Chen, Y. Liu Lian, J. Geogr. Sci. 12 (2002) 210.
[21] P. Talkner, R.O. Weber, Phys. Rev. E 62 (2000) 150.
[22] R.O. Weber, P. Talkner, J. Geophys. Res. 106 (D17) (2001) 20131.
[23] Y.H. Ding, J.C.L. Chan, Meteorol. Atmos. Phys. 89 (2005) 117.
[24] R.H. Huang, L.T. Zhou, W. Chen, Adv. Atmos. Sci. 20 (2003) 55.
[25] H.H. Hsu, X. Liu, Geophys. Res. Lett. 30 (20) (2006) 2066.
[26] C.F. Li, M. Yanai, J. Clim. 9 (1996) 358.
[27] G.X. Wu, Y.S. Zhang, Mon. Weather Rev. 126 (1998) 913.
[28] A.M. Duan, G.X. Wu, Clim. Dyn. 8 (2005) 793.
[29] Y.H. Ding, J. Meteor. Soc. Japan 70 (1992) 373.
[30] W.H. Qian, H.S. Kang, D.K. Lee, Theor. Appl. Climatol. 73 (2002) 151.
[31] X.D. Liu, M. Yanai, Int. J. Climatol. 22 (2002) 1075.
[32] B. Wang, R. Wu, X. Fu, J. Clim. 13 (2000) 1517.
[33] Y. Zhang, T. Li, B. Wang, J. Clim. 17 (2004) 2780.